ScieRxiv
NOT PEER-REVIEWED
Original Article

Preoperative Prediction of Lymph Node Metastasis in Esophageal Squamous Cell Carcinoma Using 18F-FDG PET/CT Radiomics: A Retrospective Study

Dongyuan Li[1,†], Zhenshan Wang[2,†], Huai Chen[3], Lin Hou[2,5], Haijian Huang[2,5], Guisheng Yang[2], Zhiqiang Feng[1], Yongwei Lian[1], Zhiping Lin[4], and Weipeng Huang[1,2,*]

[1]Meizhou Hospital of Guangzhou University of Chinese Medicine (Meizhou Hospital of Traditional Chinese Medicine, Meizhou Tianjiabing Hospital, Meizhou Academy of Chinese Medical Sciences), Meizhou 514000, Guangdong, China.
[2]Department of Medical Imaging Center, Jieyang People's Hospital, Jieyang 522000, Guangdong, China.
[3]The Second Affiliated Hospital of Guangzhou Medical University, Guangzhou 510000, Guangdong, China.
[4]GE Healthcare, Guangzhou 510623, Guangdong, China.
[5]Guangdong Medical University, Zhanjiang 524000, Guangdong, China.
†These authors contributed equally to this work.

Correspondence to: Prof./Dr. Weipeng Huang, Department of Medical Imaging Center, Jieyang People's Hospital, Jieyang 522000, Guangdong, China.
E-mail:jyhuangweipeng@vip.sina.com

Received: 4 September 2024 | **Approved**: 6 September 2024 | **Online**: 10 September 2024

Abstract

Aim: Lymph node (LN) metastasis is the most critical prognostic factor in esophageal squamous cell carcinoma (ESCC). This study aimed to evaluate the potential of 18F-fluorodeoxyglucose positron emission tomography/computed tomography (18F-FDG PET/CT) radiomics in predicting LN metastasis in ESCC patients.

DOI: 10.20517/scierxiv202409.05.v1

Methods: This retrospective study evaluated 129 ESCC patients who underwent radical esophagectomy and LN dissection after 18F-FDG PET/CT scans. Radiomic features were extracted from PET, CT, and combined PET+CT images, and three corresponding predictive models were constructed. The diagnostic performance of each model was assessed by measuring the area under the curve (AUC), accuracy, sensitivity, and specificity. DeLong test was employed to compare the AUC, calibration curves were used to assess model accuracy, and decision curve analysis was utilized to evaluate clinical benefit.

Results: No significant differences were observed between the training and validation cohorts regarding age, gender, tumor location, tumor stage (early vs. advanced), or differentiation grade, with respect to the presence or absence of LN metastasis (all $P>0.05$). Ten PET and nine CT radiomic features were selected from 1,688 extracted features to build the predictive models. The combined PET+CT model achieved the highest AUC, followed by the PET model and then the CT model in both training and validation cohorts (AUC: 0.883, 0.846, 0.799 in training; 0.864, 0.839, 0.736 in validation, respectively).

Conclusion: This study demonstrates the potential of PET/CT-based radiomics for preoperatively predicting LN metastasis in ESCC. While CT-based radiomics shows predictive value, PET radiomics offers superior performance. Furthermore, the combined PET+CT model demonstrates the highest diagnostic accuracy, suggesting that utilizing both imaging modalities together provides synergistic information. This non-invasive approach could potentially contribute to personalized treatment strategies and improve patient outcomes in ESCC.

Keywords: Esophageal squamous cell carcinoma, PET/CT, 18F-FDG, lymph node metastasis, radiomics, texture feature

INTRODUCTION

Esophageal cancer (EC) is a prevalent malignancy worldwide, ranking as the eighth most common cancer by incidence and the sixth leading cause of cancer-related death[1]. Esophageal squamous cell carcinoma (ESCC) is the predominant histological subtype of EC, particularly in regions such as China, where it accounts for over 50% of both incidence and mortality rates[2-5]. Approximately 90% of EC patients are diagnosed at an advanced stage, and treatment strategies for early and advanced EC differ significantly.

Early-stage EC, without lymph node metastasis (LNM), can be effectively managed with endoscopic mucosal resection or submucosal dissection. However, advanced EC, which is characterized by LNM, requires more aggressive interventions, including lymphadenectomy, radical chemoradiotherapy, and neoadjuvant chemoradiotherapy[2,3,5]. The presence of LNM significantly impacts the five-year overall survival rate, underscoring the importance of accurate staging[2,6-8].

The unique submucosal lymphatic drainage pattern of the esophagus, characterized by regional, bidirectional, and skip metastases, poses challenges for accurate LNM detection[9]. Current imaging modalities, including endoscopic ultrasound (EUS), computed tomography (CT), magnetic resonance imaging (MRI), and positron emission tomography (PET)/CT, exhibit limitations in their ability to reliably predict LNM[10,11]. EUS carries potential risks, including esophageal perforation and bleeding[12]. MRI, while valuable, requires longer examination times, and image quality can be compromised by respiration, heart rate, and peristaltic motion[13]. While PET/CT provides metabolic information, the assessment of LNM often relies on size criteria based on CT images, with lymph nodes measuring ≥10 mm in short axes typically considered metastatic. However, reports suggest[14] that when the short-axis diameter of lymph nodes is ≥10mm, the sensitivity ranges from 30% to 60%, specificity from 60% to 80%, and accuracy from 27% to 86%. This wide variability has led to considerable controversy regarding the diagnostic accuracy.

In recent years, radiomics has been proven capable of non-invasively predicting tumor heterogeneity and providing more potential information preoperatively. Its potential in predicting LNM in EC has been demonstrated in several studies using CT and MRI[15,16]. Regarding the prediction of LNM using PET images, previous research suggests that radiomics models based on 18F-fluorodeoxyglucose (FDG) PET can predict LNM in esophageal adenocarcinoma to a certain extent[17]. Therefore, this study developed and validated a PET/CT radiomic model for predicting LNM in ESCC patients by extracting the radiomic features of the tumor itself from PET/CT images.

In this study, we constructed three models: (1) a PET image-based model; (2) a co-registered CT image-based model; and (3) a combined PET+CT image-based model.

By comparing these three models, we aim to explore the value of radiomics derived from ESCC PET/CT images in predicting LNM.

METHODS

Study Population and Design

This retrospective study was approved by the Institutional Review Board of our hospital (approval number 2024010) and conducted in accordance with the Declaration of Helsinki. Informed consent was waived due to the retrospective nature of the study. We analyzed data from 129 patients diagnosed with ESCC who underwent radical esophagectomy with regional lymph node dissection between January 2019 and May 2023. All patients received 18F-FDG PET/CT scans within four weeks prior to surgery.

Inclusion and Exclusion Criteria

Patients were included if they met the following criteria: (1) thoracic ESCC with a single lesion and confirmed lymph node pathology; (2) good-quality PET/CT images with no evidence of distant metastasis on PET; and (3) no prior radiotherapy or chemotherapy. Patients were excluded if they had (1) incomplete clinical or pathological data; (2) poor quality images; (3) a history of other malignancies; or (4) received neoadjuvant radiotherapy or chemotherapy.

Data Collection and Follow-up

Clinical and pathological data were retrieved from electronic medical records and included patient demographics (age, gender), surgical records, postoperative pathology reports, and preoperative PET/CT images. All surgically resected specimens were evaluated and staged according to the 8th edition of the Union for International Cancer Control/American Joint Committee on Cancer (UICC/AJCC) tumor-node-metastasis (TNM) classification guidelines.

Image Acquisition

All patients underwent PET/CT scans using a Philips Ingenuity TF 64 PET/CT scanner (Ingenuity TF 64, Philips, Netherlands). Patients fasted for at least four to six hours before intravenous administration of 18F-FDG (provided by Guangzhou Atom High-Tech Isotope Pharmaceutical Co., Ltd. or Dongguan Andico Positron Research and Development Co., Ltd., with a radiochemical purity >95%). Blood glucose levels

were monitored before injection and maintained within the normal range (<150 mg/dL). The injected dose of 18F-FDG was 3.7-5.5 MBq/kg. Scans were acquired 60 minutes post-injection, covering the region from the vertex to the mid-thigh. CT scan parameters were as follows: tube voltage 120 kV, tube current 200 mA, pitch 0.827, collimation 64 × 0.625 mm, rotation time 0.75 s, and reconstruction slice thickness 4 mm. PET data were acquired in three-dimensional (3D) mode with 9-11 bed positions, each with an acquisition time of 1.5 minutes. PET images were reconstructed using the ordered subset expectation maximization (OSEM) algorithm, and CT images were reconstructed using a standard algorithm.

Tumor Delineation

Tumor volumes of interest (VOIs) were manually delineated on both PET and CT images using ITK-SNAP software (version 3.6.0, http://www.itksnap.org). A senior radiologist with six years of experience contoured the tumor on each slice of the PET image (threshold set at approximately 40%) and the corresponding CT image (window width 300 HU, window level 40 HU), carefully avoiding inclusion of esophageal air or adjacent structures. The delineations were reviewed and revised by a deputy chief radiologist with over ten years of experience. In cases of disagreement, a chief radiologist with over 20 years of experience was consulted to reach a consensus. The tumor delineation process is illustrated in Figure 1.

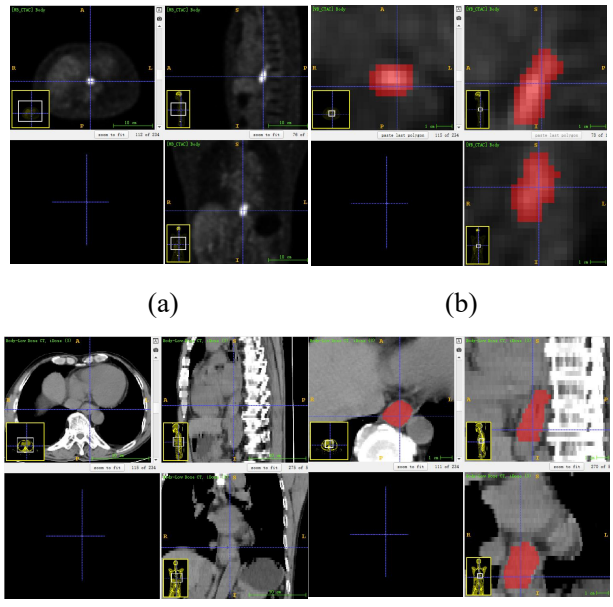

(a) (b)

(c) (d)

Figure 1. Illustration of the tumor delineation process. (a) 3D reconstructed PET image,

with the tumor highlighted by adjusting the optimal threshold. (b) Zoomed-in view of the tumor region, with manual contouring performed slice-by-slice on the PET image to generate the VOI. (c) and (d) Similar process for delineating the tumor VOI on the CT image using the optimal window width and level.

Radiomic Feature Extraction and Selection

A total of 1,688 radiomic features were extracted from both PET and CT images using the Pyradiomics Python package. These features included morphological, first-order, textural, and wavelet-transformed features. Feature dimensionality reduction and selection were performed using the minimum redundancy maximum relevance (mRMR) and least absolute shrinkage and selection operator (LASSO) algorithms. Ten-fold cross-validation was used to determine the optimal lambda value for the LASSO regression model. Features with non-zero coefficients at the optimal lambda value were selected for model construction. A radiomics score (Radscore) was calculated as the sum of the product of each retained feature and its corresponding coefficient. The combined PET+CT model was generated using a linear weighted combination of the Radscore from PET and Radscore from CT.

Model Development and Validation

The cohort was randomly divided into a training set (n=91) and a validation set (n=38) using a 7:3 ratio. Three separate radiomic models were developed using binary logistic regression (LR) algorithms: a PET-based model, a CT-based model, and a combined PET+CT model. The performance of each model was evaluated using the validation set. The workflow of the radiomics analysis is presented in Figure 2.

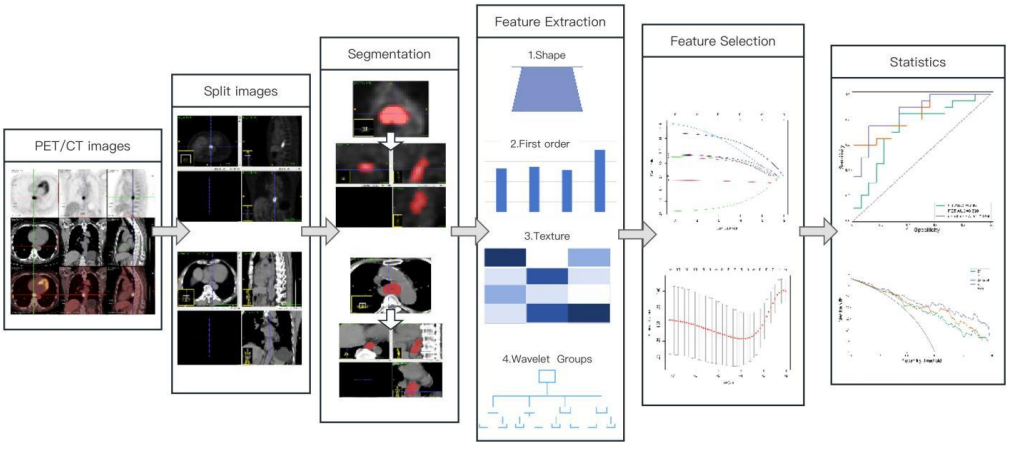

Figure 2. Workflow of the radiomics analysis. The original PET/CT images were

separated into PET and CT components. Manual delineation and segmentation were performed to generate tumor VOIs. Radiomic features, including shape, first-order histogram, texture features, and wavelet-transformed features, were extracted from the VOIs. Feature dimensionality reduction and selection were conducted using mRMR and LASSO regression to identify the optimal features for model building. Finally, the performance of the models was evaluated using statistical analysis.

Statistical Analysis

Statistical analysis was performed using SPSS 26.0 software. The Shapiro-Wilk test was used to assess the normality of continuous variables. Normally distributed data were presented as mean ± standard deviation (SD), and non-normally distributed data were presented as median (interquartile range). Categorical data were analyzed using the Fisher's exact test or chi-square test. Receiver operating characteristic (ROC) curve analysis was used to evaluate the diagnostic performance of the prediction models. The area under the ROC curve (AUC), accuracy, sensitivity, and specificity were calculated. The DeLong test was used to compare the AUCs of the three models. Decision curve analysis was used to assess the clinical utility of the models. A p-value of < 0.05 was considered statistically significant.

RESULTS

Patient Characteristics

A total of 129 patients diagnosed with ESCC who underwent 18F-fluorodeoxyglucose (18F-FDG) PET/CT scans followed by esophagectomy with lymph node dissection were included in this retrospective study. Patients were randomly divided into a training cohort (n=91) and a validation cohort (n=38). No significant differences were observed between the two cohorts in terms of age, gender, tumor stage, tumor location (upper, middle, or lower thoracic esophagus), or tumor differentiation grade (all $P > 0.05$), suggesting comparable baseline characteristics. Detailed patient demographics and clinical characteristics are presented in Table 1.

DOI: 10.20517/scierxiv202409.05.v1

Table 1. Clinicopathological Characteristics of Patients in the Training and Validation Cohorts

Characteristics	Training Cohort				Validation Cohort			
	Negative (n = 42)	Positive (n = 49)	t/χ2	P value	Negative (n = 16)	Positive (n = 22)	t/χ2	P value
Age (y), mean ± SD	67.45 ± 7.37	65.10 ± 7.64	1.49	0.140	67.62 ± 6.17	67.45 ± 6.25	0.08	0.934
Gender, no.(%)			0.00	0.945			-	0.267
Female	14 (33.33)	16 (32.66)			6 (37.50)	4 (18.18)		
Male	28 (66.67)	33 (67.35)			10 (62.50)	18 (81.82)		
Pathological T stage, no.(%)			0.13	0.715			-	0.075
T1/T2	9 (21.43)	9 (18.37)			8 (50.00)	4 (18.18)		
T3/4a	33 (78.57)	40 (81.63)			8 (50.00)	18 (81.82)		
Tumor location, no.(%)			-	0.732			-	0.881
Lower	3 (7.14)	5 (10.20)			1 (6.25)	2 (9.09)		

DOI: 10.20517/scierxiv202409.05.v1

Middle	26 (61.90)	26 (53.06)			10 (62.50)	11 (50.00)		
Upper	13 (30.95)	18 (36.73)			5 (31.25)	9 (40.91)		
Differentiation degree, no.(%)			0.40	0.820			-	0.097
Poorly	14 (33.33)	14 (28.57)			5 (31.25)	1 (4.55)		
Moderately	22 (52.38)	26 (53.06)			7 (43.75)	14 (63.64)		
Well	6 (14.29)	9 (18.37)			4 (25.00)	7 (31.82)		

DOI: 10.20517/scierxiv202409.05.v1

Radiomics Feature Extraction and Model Development

A total of 1,688 radiomics features were extracted from both PET and CT images, encompassing morphological, first-order, textural, and higher-order wavelet transformed features. Feature selection was performed using the LASSO regression algorithm. Following dimensionality reduction, ten PET and nine CT features were retained for model construction (Figure 3). The selected features and their corresponding coefficients are listed in Tables 2 and 3. These features were then used to build three distinct LR models: a PET-based model, a CT-based model, and a combined PET+CT model. The combined model employed a linear weighting of the Radscores derived from the individual PET and CT models, represented by the equation: Radscore = 1.33380049 * PET + 1.01324718 * CT - 0.2671535. The optimal cutoff values for predicting LNM were determined using Youden's index and were calculated to be 0.657 for the CT model, 0.612 for the PET model, and 0.661 for the combined PET+CT model.

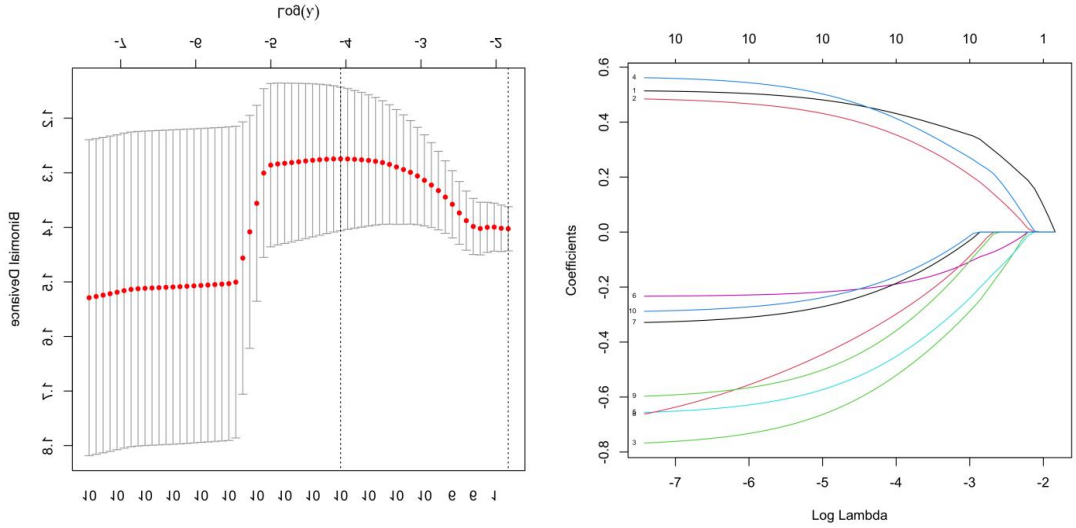

(a) (b)

Figure 3. Feature Selection Process. (a) Binomial deviance plotted against the optimal hyperparameter log(λ) using LASSO regression. (b) LASSO convergence coefficients for different texture features, highlighting the ten PET features with non-zero coefficients.

DOI: 10.20517/scierxiv202409.05.v1

Table 2. Selected PET Radiomics Features and Their Coefficients

PET Radiomics Feature	Coefficient
wavelet_HLL_glszm_SmallAreaEmphasis	-0.580
gradient_glszm_SmallAreaLowGrayLevelEmphasis	-0.503
wavelet_LHH_glcm_MaximumProbability	-0.419
logarithm_ngtdm_Coarseness	-0.354
wavelet_HHL_glrlm_LowGrayLevelRunEmphasis	-0.223
squareroot_glszm_SmallAreaEmphasis	-0.203
lbp_3D_k_ngtdm_Strength	-0.195
logarithm_glcm_ClusterShade	0.387
wavelet_LLH_glrlm_RunVariance	0.450
wavelet_LLH_firstorder_Mean	0.452

Table 3. Selected CT Radiomics Features and Their Coefficients

CT Radiomics Feature	Coefficient
wavelet_HHL_gldm_SmallDependenceLowGrayLevelEmphasis	-0.458
wavelet_HLH_ngtdm_Strength	-0.084
wavelet_LHH_glszm_SmallAreaEmphasis	0.239
logarithm_firstorder_Maximum	0.253
lbp_3D_k_firstorder_Skewness	0.255
wavelet_HLH_glszm_SmallAreaLowGrayLevelEmphasis	0.259
wavelet_HLH_glcm_MaximumProbability	0.279
wavelet_LLH_glszm_LargeAreaLowGrayLevelEmphasis	0.481
wavelet_HHL_firstorder_Skewness	0.565

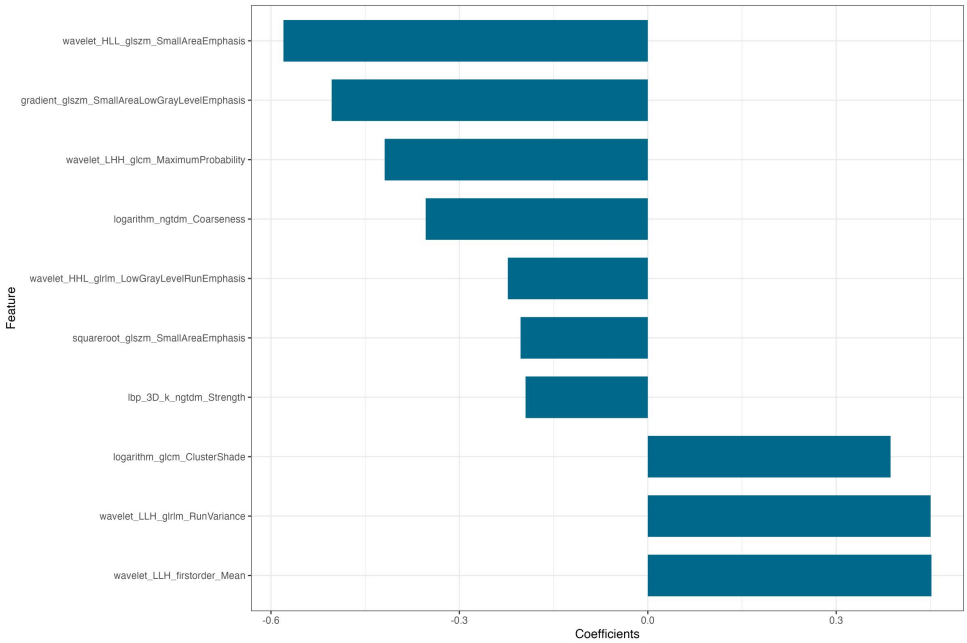

(a)

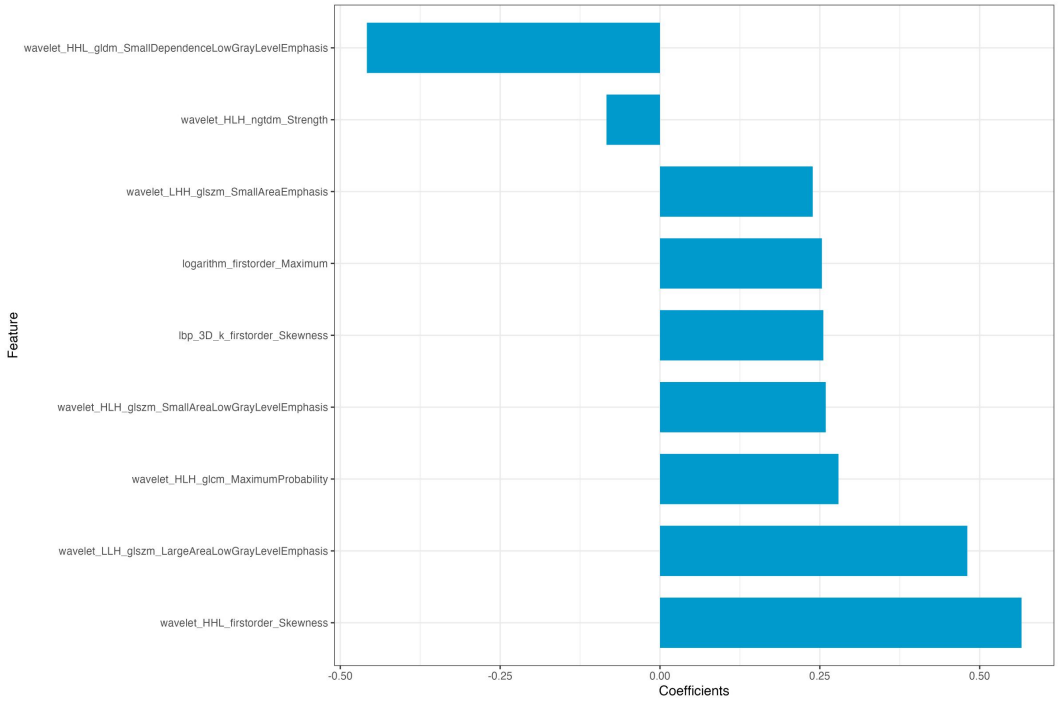

(b)

Figure 4. Selected Features and Their Corresponding Coefficients in the Radiomics Models. (a) Ten features and their coefficients incorporated in the PET radiomics model. (b) Nine features and their coefficients incorporated in the CT radiomics model.

Evaluation of Model Performance

The performance of the three radiomics models was evaluated using ROC curve analysis (Figure 5). The AUC, accuracy, sensitivity, and specificity for each model are summarized in Table 4. The DeLong test revealed no statistically significant differences in AUC values among the three models in the validation cohort (all $P > 0.05$). However, in the training cohort, the PET+CT model demonstrated a significantly higher AUC compared to the CT model ($P = 0.02$), while the difference between the PET+CT and PET models was not significant ($P > 0.05$). Calibration curves (Figure 6) indicated good agreement between predicted and actual probabilities for all three models in both training and validation cohorts ($P > 0.05$), with the PET+CT model exhibiting the closest adherence to the ideal calibration line. Decision curve analysis (Figure 7) demonstrated that all three models provided clinical benefit to patients, with the PET+CT model offering the highest net benefit. Further analysis using net reclassification improvement (NRI) and integrated discrimination improvement (IDI) (Table 5) confirmed the superior performance of the PET+CT

model, demonstrating its ability to improve risk stratification compared to the individual PET and CT models.

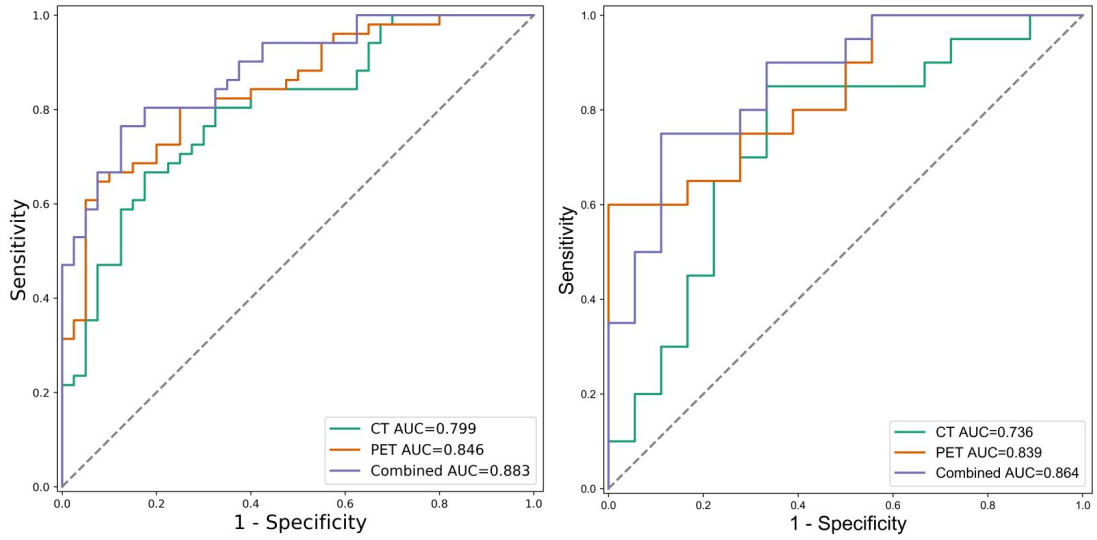

(a) (b)

Figure 5. ROC Curves for the CT, PET, and Combined PET+CT Radiomics Models. (a) Training cohort. (b) Validation cohort.

Table 4. Performance Metrics of the Three Radiomics Models in the Training and Validation Cohorts

Model	Training Cohort（n=91）				Validation Cohort (n=38)			
	AUC (95%CI)	Accuracy (95%CI)	Sensitivity (95%CI)	Specificity (95%CI)	AUC (95%CI)	Accuracy (95%CI)	Sensitivity (95%CI)	Specificity (95%CI)
PET	0.846(0.765, 0.921)	0.758(0.661, 0.834)	0.627(0.490, 0.746)	0.925(0.801, 0.974)	0.839(0.703, 0.939)	0.737(0.580, 0.850)	0.650(0.433, 0.819)	0.833(0.607, 0.941)
CT	0.799(0.707, 0.886)	0.725(0.626, 0.806)	0.647(0.510, 0.764)	0.825(0.680, 0.913)	0.736(0.565, 0.899)	0.632(0.473, 0.767)	0.450(0.258, 0.658)	0.833(0.607, 0.941)
Combined Model	0.883(0.810, 0.938)	0.802(0.709, 0.871)	0.745(0.611, 0.844)	0.875(0.739, 0.945)	0.864(0.721, 0.967)	0.789(0.636,0.889)	0.700(0.481,0.855)	0.889(0.672,0.969)

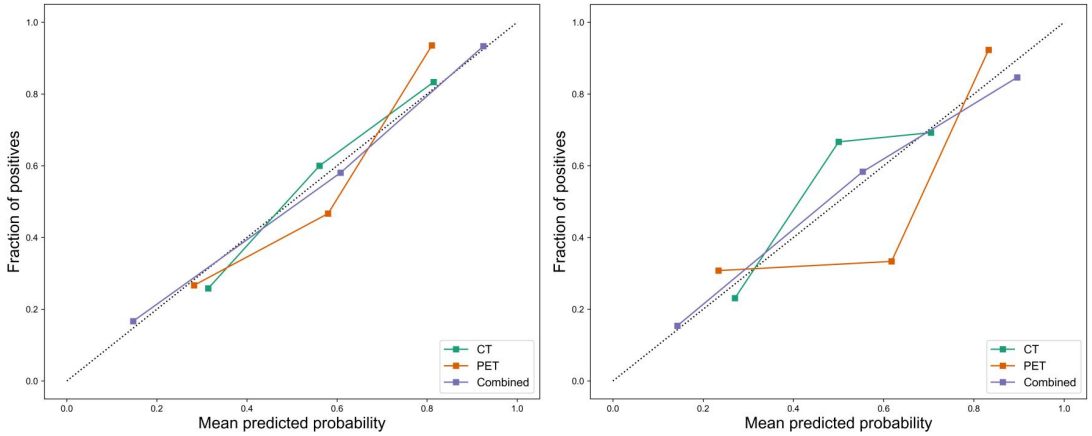

(a) (b)

Figure 6. Calibration Curves for the CT, PET, and Combined PET+CT Radiomics Models. (a) Training cohort. (b) Validation cohort. The 45-degree line represents perfect calibration.

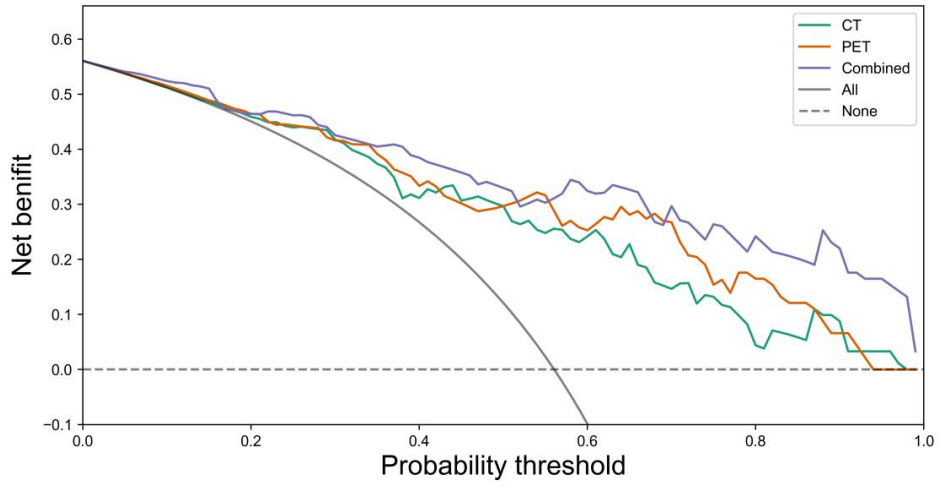

(a)

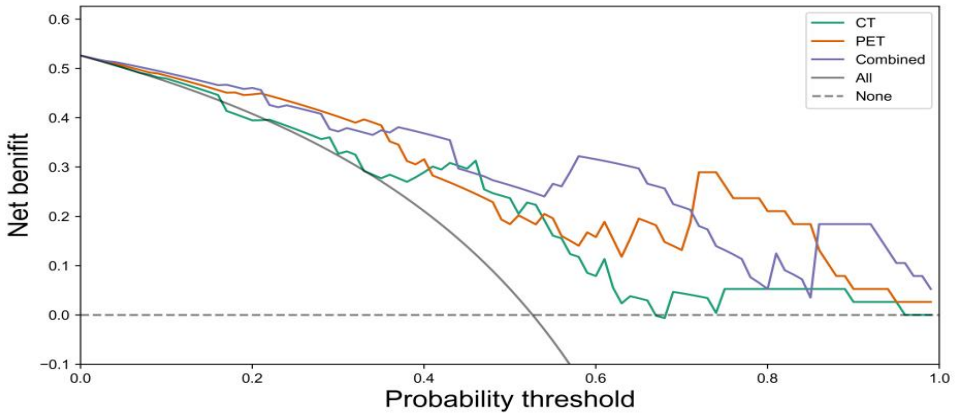

(b)

Figure 7. Decision Curves for the CT, PET, and Combined PET+CT Radiomics Models. (a) Training cohort. (b) Validation cohort.

Table 5. Continuous NRI and IDI for Model Performance Comparison

Model Comparison	Training Cohort (n=91)		Validation Cohort (n=38)	
	NRI (95%CI)	IDI (95%CI)	NRI (95%CI)	IDI (95%CI)
PET vs. CT	-0.100[-0.325,-0.125]	-0.062[-0.163,-0.038]	-0.144[-0.527,-0.239]	-0.160[-0.344, -0.023]
Combined vs. PET	0.048[-0.110,-0.206]	0.144[0.084,-0.204]	0.211[0.015, -0.407]	0.095[0.005, -0.184]
Combined vs. CT	0.148[-0.024,-0.320]	0.206[0.130,-0.282]	0.356[0.018, -0.693]	0.255[0.109, -0.401]

DISCUSSION

This study investigated the potential of 18F-FDG PET/CT radiomics in predicting LNM in patients with ESCC. By delineating the 3D VOI of the esophageal tumor, we were able to capture more comprehensive and accurate information compared to traditional two-dimensional regions of interest (ROI). We developed and compared three distinct models: one based solely on PET images, another on co-registered CT images, and a final model combining features from both PET and CT. Our results demonstrate the promising capability of 18F-FDG PET/CT radiomics in preoperatively predicting LNM in ESCC.

Lymph node status is a critical prognostic factor in ESCC[6,7,8], directly influencing tumor staging, surgical planning, and, ultimately, patient outcomes. Previous research has focused mainly on CT-based radiomics for predicting LNM in ESCC. Liu et al.[18] highlighted the utility of texture features in differentiating metastatic from non-metastatic lymph nodes, while Ou et al.[19] and Shen et al.[20] demonstrated the predictive capabilities of CT radiomics models. Although the combined nature of PET/CT theoretically provides richer information than CT alone, its application in radiomics has predominantly been confined to evaluating treatment response and prognosis[21-25]. Therefore, this study aimed to address this gap by developing and evaluating separate PET and CT radiomics models and, subsequently, a combined PET/CT model, to determine the unique advantages of incorporating PET data for LNM prediction in ESCC.

Our study identified ten optimal PET and nine optimal CT radiomics features for model construction. The PET features included one higher-order transformed

first-order feature and nine texture features, while the CT features consisted of three higher-order transformed first-order features and six texture features. This selection aligns with previous research[26] indicating the ability of first-order statistical and texture features to accurately differentiate benign and malignant mediastinal lymph nodes. In our models, texture features were prominent in both PET and CT, showing substantial weight in the weight histograms. Notably, the PET model incorporated a greater number of these features than the CT model. Specifically, the wavelet_HLL_glszm_SmallAreaEmphasis feature held the highest weight in the PET model, demonstrating a negative correlation with LNM. This feature, derived from the Gray Level Size Zone Matrix (GLSZM)[27], reflects the calculation of contiguous voxel or pixel regions within the image. It encompasses aspects of regional homogeneity and variation, with more homogenous matrices exhibiting a wider and flatter distribution. As SmallAreaEmphasis measures the distribution of small-sized regions, a higher degree of heterogeneity – and thus, a less uniform matrix – could indicate a greater likelihood of LNM. In contrast, the wavelet_HHL_firstorder_Skewness feature, representing the skewness of the distribution about the mean, carried the highest weight in the CT model. This discrepancy from Liu et al.'s[18] findings, which identified entropy as an independent prognostic factor for LNM in ESCC, could be attributed to their use of contrast-enhanced CT images, whereas our study used non-contrast CT images acquired as part of the PET/CT protocol. Ou et al.[19] developed a CT-based radiomics model to differentiate regional LNM (RLNM) from non-regional LNM (NRLNM) in 334 patients with advanced ESCC, achieving AUCs of 0.79 and 0.75 in the training and validation cohorts, respectively. Our CT model yielded comparable AUC values of 0.799 and 0.736. Dong et al.[28] investigated the relationship between texture features and tumor stage using pre-treatment 18F-FDG PET images from 40 ESCC patients, finding correlations between energy, entropy, and tumor N stage. While our study also highlights the association between texture features and LNM, the specific features identified may differ due to the broader scope of texture features considered in radiomics analysis. Zhang et al.[17] constructed a model based on nine 18F-FDG PET radiomics features, including gray-level co-occurrence matrices (GLCM) and intensity features, to predict LNM in 190 esophageal adenocarcinoma patients, achieving AUCs of 0.79 and 0.65 in the training and external validation cohorts,

respectively. Our study, employing ten features – including GLCM, gray-level run length matrices (GLRLM), GLSZM, and neighborhood gray-tone difference matrices (NGTDM) – derived from 18F-FDG PET images of ESCC patients, achieved higher AUC values of 0.846 and 0.839. This suggests that 18F-FDG PET-based radiomics models may have the potential to predict LNM across various histopathological subtypes of EC, likely due to the ability of radiomics features to capture tumor heterogeneity relevant to metastatic processes.

In recent studies, there has been a growing focus on using PET/CT and CT imaging to predict LNM in EC patients. Jayaprakasam et al.[29] studied the 18F-FDG PET/CT imaging features to predict the clinical prognosis of patients with locally advanced ESCC. They compared the AUC, accuracy, sensitivity and specificity of the CT, PET and combined PET+CT models. All three radiomics models perform well in predicting N stages. On this basis, our study also compared the calibration curve, decision curve, NRI and IDI classification efficiency of the three models. We further analyzed and compared their diagnostic efficiency and clinical benefit to increase the reliability of the results. Lei et al.[30] extracted the imaging features of preoperative PET/CT images of 100 patients with ESCC, and constructed the prediction models using PET, CT, fused PET-CT images and combined PET+CT images. They found that PET/CT imaging could accurately predict ESCC staging, and that for N staging, models combining CT and PET radiomics features showed the best predictive performance, with AUC values of 0.918 and 0.824 in the training and validation cohorts, respectively. In this study, the AUC values for the training and verification cohorts of the combined model were 0.883 and 0.864, respectively, showing consistency with Lei et al.'s findings. However, Lei et al. concluded that single CT imaging performed better than single PET imaging, with AUCs of 0.883 vs. 0.780 in the training cohort and 0.769 vs. 0.760 in the validation cohort. Conversely, our study revealed that single PET imaging outperforms single CT imaging, consistent with the study of Jayaprakasam et al[29]. This discrepancy may be because CT images mainly provide structural information, and have advantages in extracting morphological features, whereas PET images reflect functional and metabolic information, potentially revealing features directly related to disease states that may not be evident on CT images. Therefore, it can be inferred that in imagomics analysis, PET imaging

may extract more comprehensive and characteristic features than CT, especially concerning functional and metabolic changes in disease. The differing results from Lei[30] may be due to their smaller sample size of only 100, which could lead to unstable estimates. Similarly, our study included only 129 patients. Therefore, future studies should include larger sample sizes to enhance the reliability and validity of the results. Furthermore, the higher AUC observed for texture features compared to first-order features aligns with the understanding that texture features are more adept at capturing spatial heterogeneity within the tumor microenvironment. First-order features, which primarily reflect the distribution of pixel intensity values, lack the spatial context needed to evaluate the intricate spatial relationships and heterogeneity patterns within the tumor[31,32]. The combined PET+CT model consistently achieved the highest AUC in both training and validation cohorts. This is likely due to the integration of CT-derived features (including first-order, second-order, texture, and wavelet features) with PET-specific metabolic parameters such as standardized uptake value (SUV), metabolic tumor volume (MTV), and total lesion glycolysis (TLG). By incorporating this comprehensive set of features, the combined model provides a more holistic characterization of tumor characteristics associated with LNM, resulting in enhanced diagnostic accuracy. This combined PET+CT model essentially reflects the clinical application of PET/CT imaging.

This study has certain limitations that should be acknowledged. First, its retrospective, single-center design requires further validation through prospective, multi-center studies. Second, our analysis focused on radiomic features extracted from the primary tumor, and future research could explore the potential of incorporating radiomic features derived from the lymph nodes themselves. Third, PET metabolic parameters such as SUV, MTV, and TLG were not included in the current model construction, and future studies could investigate the potential benefits of incorporating these parameters into the radiomics analysis. Finally, external validation is crucial to confirm the robustness and generalizability of the developed models.

Conclusion

This study demonstrates the potential of a novel, non-invasive PET/CT-based radiomics model for predicting LNM in ESCC. By analyzing PET and CT

components separately, we preliminarily suggested the superior performance of PET-derived radiomic features in capturing tumor heterogeneity and predicting LNM. Furthermore, the integrated PET/CT model exhibited enhanced predictive accuracy compared to the individual modalities, suggesting its potential clinical utility in guiding preoperative staging and personalized treatment strategies for ESCC patients. These findings warrant further investigation and validation in larger, multi-center studies.

DECLARATIONS

Acknowledgments

We thank the open source software ITK-SNAP for providing the sketching tool (http://www.itksnap.org). We also express our gratitude to the open source software Python package (Pyradiomics) for providing a reference to the radiomics features (http://pyradiomics.readthedocs.io).

Authors' contributions

Designed the study: Li D, Wang Z, Huang W

Processed the images: Hou L, Huang H, Feng Z, Lian Y

Statistical analysis: Lin Z, Yang Gui

Supervised the study: Chen H, Huang W

All the authors analyzed and interpreted the data, wrote, reviewed, and/or revised the manuscript, and approved the submitted version.

Availability of data and materials

The data originated from the Department of Medical Imaging Center at Jieyang People's Hospital.

Conflicts of interest

All authors declare that there are no conflicts of interest.

Financial support and sponsorship

This work was supported by the Guangdong Provincial Medical Research Fund Project (Grant No. A2024780) and the Beijing Medical Award Foundation "Ruiying

Scientific Research Fund Phase VI" Outstanding Project.

Ethical approval and consent to participate

This retrospective study was approved by the Institutional Review Board of our hospital (approval number 2024010) and conducted in accordance with the Declaration of Helsinki. Informed consent was waived due to the retrospective nature of the study.

Consent for publication

Not applicable.

Copyright

REFERENCES

1. Bray F, Ferlay J, Soerjomataram I, et al.Global cancer statistics 2018:GLOBOCAN estimates of incidence and mortality worldwide for 36 cancers in 185 countries. *CA Cancer J Clin* 2018;68:394-424.
2. Chen TW, Wu YP. Review and prospects of new progress in intelligent imaging research on lymph node metastasis in esophageal carcinoma. *West Med* 2023;4:469-473+479. (in Chinese)
3. Dan G , Yu ping W, Tian-Wu C. Review and prospects of new progress in intelligent imaging research on lymph node metastasis in esophageal carcinoma. *Meta-Radiology* 2024;2:100081.
4. Wang QL, Xie SH, Wahlin K, et al.Global time trends in the incidence of esophageal squamous cell carcinoma.*Clin Epidemiol* 2018;10:717-728
5. Zeng H, Chen W, Zheng R, et al. Changing cancer survival in china during 2003-15: a pooled analysis of 17 populationbased cancer registries. *Lancet Glob Health* Health 2018;6:e555-e567.
6. Rice TW, Ishwaran H, Hofstetter WL, et al. E-sophageal cancer: associations with (pN+) Lymph node Me- tastases. *Ann Surg* 2017:265:122-129.
7. BorggreveO A S, Kingmab F, Domrachev S A, et al. Surgical treatment of esophageal cancer in the era of multi- modality management. *Ann N Y Acad Sci* 2018:1434:192-209.

8. Furukawa T, Hamai Y, Hinara J, et al. Clinical sig-nificance of FDG-PET to predictpathologic tumor invasion and lymph node metastasisof superficialesophageal squamous cell carcinoma. *Ann Surg Oncol* 2016;23:4086-4092.
9. Fan BS, Song WA, Gong TQ. Research progress on the regularity and prediction model of lymph node metastasis of esophageal cancer. *Chin J Min Invasive Surg* (Electronic Edition) 2020;3:188-192. (in Chinese)
10. Giganti F, Amrosi A, Petrone MC, et al. Prospective comparison of MR with diffusion-weighted imaging, endoscopic ultrasound, MDCT and positron emission tomography-CT in the pre-operative staging of oesophageal cancer: results from a pilot study. *Br J Radiol* 2016;89:20160087.
11. Yang RH, Liao YT, Fan WX, et al. Predictive value of MRI-based radiomics model for lymph node metastasis of esophageal cancer. *Int J Med Radiol* 2022;6:626-631. (in Chinese)
12. Expert consensus on the application of artificial intelligence in the clinical diagnosis and treatment of esophageal cance. *Chin J Interv Radiol* (Electronic Edition) 2021;3:235-246. (in Chinese)
13. Chinese Medical Association Radiology Branch Abdominal Group. Expert consensus on the standardized application of MRI technology and structured reporting for esophageal cancer. *Chin J Radiol* 2023;8:836-43. (in Chinese)
14. PanebiancoV, Grazhdani H, lafrate F, et al. 3D CT protocol in the assessment of the esophageal neoplastic lesions: can it improve TNMstaging? *Eur Radiol* 2006;16:414-421.
15. Shen C, Liu Z, Wang Z, et al. Building CT radiomics based nomogram for preoperative esophageal cancer patients lymph node metastasis prediction. *J.Trans Oncol* 2018;11:815-24.
16. Qu J, Shen C, Qin J, et al. The MR radiomic signature can predict preoperative lymph node metastasis in patients with esophageal cancer. *Eur Radiol* 2019;29:906-14.
17. Zhang C, Shi Z, Kalendralis P, et al. Prediction of lymph node metastases using pre-treatment PET radiomics of theprimary tumour in esophageal adenocarcinoma: an external validation study. *Br J Radiol* 2021;94:20201042.

18. Liu S, Zheng H, Pan X, et al. Texture analysis of CT imaging for assessment of esophageal squamous cancer aggressiveness. *J Thorac Dis* 2017;9:4724-4732.
19. Ou J, Wu L, Li R, et al. CT radiomics features to predict lymph node metastasis in advanced esophageal squamous cell carcinoma and to discriminate between regional and non-regional lymph node metastasis: a case control study. *Quant Imaging Med Surg* 2021;11:628-40.
20. Shen C, Liu Z, Wang Z, et al. Building CT radiomics based nomogram for preoperative esophageal cancer patients lymph node metastasis prediction. *Trans Oncol* 2018;11:815-24.
21. Yang HX, Ji AB, Song SL. Research status, progress and clinical application of PET/CT radiomics. *Tumor Imaging* 2021;6:450-58. (in Chinese)
22. Gao C, Sun YY, Sun XL. Research progress and clinical application of radiomics in ~(18)F-FDG PET/CT. *Chin J Med Imaging Technol* 2020;8:1239-42. (in Chinese)
23. Chen W, Nie SD, Song SL. Research progress of artificial intelligence-based PET/CT radiomics in clinical diagnosis and treatment of tumors. *Tumor Imaging* 2021;6:433-38. (in Chinese)
24. Tixier F, Le Rest CC, Hatt M, et al. Intratumor heterogeneity characterized by textural features on baseline 18F-FDG PET images predicts response to concomitant radiochemotherapy in esophageal cancer. *J Nucl Med* 2011;52:369-78.
25. Beukinga R J, Hulshoff J B, Van Dijk L V, et al. Predicting response to neoadjuvant chemoradiotherapy in esophageal cancer with textural features derived from pretreatment (18)F-FDG PET/CT imaging. *J Nucl Med* 2017;58:723-9.
26. Bayanati H, E Thornhill R, Souza CA, et al. Quantitative CT texture and shape analysis: Can itdifferentiate benign and malignant mediastinal lymph nodes in patients with primary lung cancer?. *Eur Radiol* 2015;25:480-487.
27. Thibault G, Fertil B, Navarro C,Pereira S,Levy N, Sequeira J, Mari JL.Texture indexes and gray level size zone matrix application to cell nuclei classification. In Pattern Recognition and Information Processing, 2008.
28. Dong X, Xing L, Wu P, et al. Three-dimensional positron emission tomography image texture analysis of esophageal squamous cell carcinoma: relationship

between tumor 18F-fluorodeoxyglucose uptake heterogeneity, maximum standardized uptake value, and tumor stage. *Nucl Med Commun* 2013;34:40-46.

29. Jayaprakasam VS, Gibbs P, Gangai N, et al. Can 18F-FDG PET/CT radiomics features predict clinical outcomes in patients with locally advanced esophageal squamous cell carcinoma?. *Cancers* 2022;14:3035.
30. Lei X, Cao Z, Wu Y, et al. Preoperative prediction of clinical and pathological stages for patients with esophageal cancer using PET/CT radiomics. *Insights Imaging* 2023;14:174.
31. Li G, Zhai G, Zhao X, et al. 3D texture analyses within the substantia nigra of Parkinson's disease patients on quantitative susceptibility maps and R2 maps. NeuroImage, 2019;188:465-472.
32. Xia XD, Duan CZ, Wang GX, et al. Prediction of axillary lymph node metastasis in breast cancer by MRI texture analysis. *Chin J Med Imaging Technol* 2021;4:531-36. (in Chinese)